Electronic Detection of Photonic Band Gaps in Nanolithographic Metallic Gratings

William T. Rieger, Jr., Yuhong Kang, Jean J. Heremans, and Hang Ruan

Abstract— **In nanolithographic metallic gratings we investigate the dependence of photonic band gaps on geometrical parameters. Finite element modeling was used to develop a model for an optoelectronic device with periodicity of 470 nm and concomitantly the electronic response of a nanofabricated metal-semiconductor-metal photodetector grating was experimentally studied under a sweeping monochromatic light source. The grating spectral response increased in the region between 470 nm and 520 nm, corroborating the computational results. This increase is understood to occur because photons with wavelength shorter than approximately 520 nm are energetic enough to excite interband transitions in the Au, but the period of the structure acts as a cutoff where incident photons with wavelength shorter than the period are less likely to form surface plasmon polaritons. This cutoff originates from a photonic band gap. Magnetic field intensity profiles at the 3 dB cutoff indicate that a surface plasmon wave exists where each finger interacts with the next through overlapping magnetic fields, suggesting that the cutoff is a surface plasmon wave effect. Localized surface plasmon effects were observed at longer wavelengths in the modeled absorbance. The effects of three geometrical parameters on the spectral dependence of modeled absorbance were investigated.**

Index Terms— **Plasmon, optoelectronic devices, metallic grating, photonic band gap.**

I. Introduction

SUBWAVELENGTH structures are of interest due to their ability to engineer material properties beyond the limits of naturally occurring compounds. Current nanofabrication techniques allow the development of geometry-enhanced devices operating in the visible and infrared region of the spectrum. Specifically, hyperbolic metamaterials [1]–[3], negative indices of refraction [4], [5], second harmonic generation [6], [7], and photonic crystals [8]–[12] have all been of interest. The metallic grating studied here functions as a 1-dimensional (1D) photonic crystal. Metallic gratings with sub-wavelength slits have been studied previously using optical techniques [13]–[15]. The present work presents an electrical characterization based on our previously reported technique [16]. By comparing the electrical measurement with modeled plasmonic excitations we highlight the mechanisms that contribute to the electronic signal. We report an electrical detection of photonic band gaps and computational analysis of a metallic grating fabricated on a semiconductor surface where Schottky barriers are formed at the structure-semiconductor interface. Such a structure is a metal-semiconductor-metal (MSM) electronically rectifying detector device that exhibits an open circuit voltage, V_{oc}, when the metallic grating is photoexcited. Spectral response of traditional MSM detectors is determined by the material properties of the semiconducting substrate. In metallic gratings on the other hand, if the surface structure interacts with incident light of wavelength comparable to its periodicity, then the spectral response is a function of this periodicity, yielding a modifiable spectral response characteristic of a 1D photonic crystal. Previous work indicates that the dispersion relation of a surface plasmon polariton (SPP) exhibits a band gap [8]–[12], [17]–[20]. The wavelengths marking the edge of the band gap are expressed as [9]:

$$\left(\frac{2\pi}{\lambda_{\mp}}\right)^2 = \left(\frac{2\pi}{\lambda_0}\right)^2 [1-(Kd)^2] \pm 2(Kd)\frac{K^2}{\sqrt{-\epsilon_m \epsilon_d}}[1-(Kd)^3] \quad (1)$$

where $2K$ represents the Bragg wave vector, d the amplitude of the surface corrugation (equivalent to $T/2$ as defined below), λ_0 the wavelength of the free space photon, $\lambda_{\mp}$ the upper and lower band edges as wavelengths, ϵ_m, and ϵ_d relative permittivity of the metal and dielectric respectively. This analytical expression suggests the existence of a band gap, but cannot be readily solved for our device due to a discontinuity in the Au permittivity at approximately 500 nm [21]. We hence use computational techniques to ascertain the location of the band gap. Further, electrical measurements provide experimental evidence of the band gap through the following process. Monochromatic light couples to surface plasmon modes forming SPPs on the metal structure. Surface plasmon waves (SPW) on a uniform thin metal film may exist freely, and it is the relative permittivities of the two materials that determine the conditions necessary for an SPP. Alternatively, localized surface plasmons (LSP) can exist on nanostructures such as nanospheres, nanorods, and nanoantennas; these may

Manuscript received February 6, 2020; revised April 1, 2020; accepted April 21, 2020. Date of publication May 6, 2020; date of current version May 18, 2020. This work was support by the U.S. Navy under Contract N68335-13-C-0184. *(Corresponding author: Hang Ruan.)*

William T. Rieger, Jr., is with the Department of Physics, Virginia Tech, Blacksburg, VA 24061 USA, and also with NanoSonic Inc., Pembroke, VA 24136 USA.

Yuhong Kang is with NanoSonic Inc., Pembroke, VA 24136 USA.

Jean J. Heremans is with the Department of Physics, Virginia Tech, Blacksburg, VA 24061 USA.

Hang Ruan is with NanoSonic Inc., Pembroke, VA 24136 USA, and also with the Department of Mechanical Engineering, Virginia Tech, Blacksburg, VA 24061 USA (e-mail: hruan@nanosonic.com).

Color versions of one or more of the figures in this article are available online at http://ieeexplore.ieee.org.

Digital Object Identifier 10.1109/JQE.2020.2992761

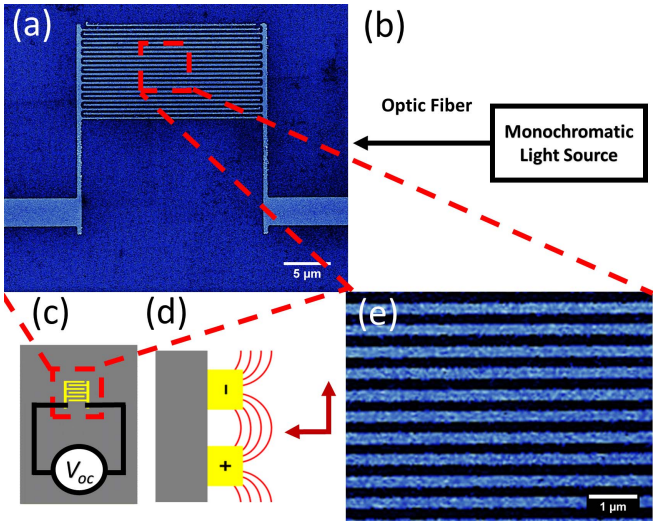

Fig. 1. Nanolithographic metallic grating device and characterization technique. a) Nanolithographic metallic grating and macroscopic electrodes. b) Experimental measurement setup. c) Electrical characterization schematic. The open circuit voltage (V_{oc}) is measured between any two adjacent interdigitated fingers. d) Illustration of one selected resonance leading to an increased open circuit voltage e) Scanning electron micrograph of the nanolithographic metallic grating.

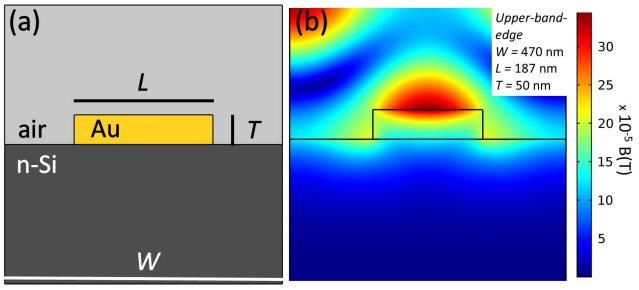

Fig. 2. 2D finite element modeling using COMSOL software. (a) Geometry for the 2D finite element modeling. Ports exist at the upper and lower boundaries with monochromatic p-polarized light originating at the upper boundary and normally incident on the grating. Periodic boundary conditions are used at the left and right boundaries. (b) Total magnetic field intensity profile at upper-band-edge. False color is magnetic field intensity.

also couple with incident photons forming an SPP. Both SPW and LSP exist in the present grating. Overall periodicity has a larger impact on SPW; structural details at the cross sections have a larger role in LSP. The effect of the grating dimensional parameters on both SPW and LSP are considered. We relate measured V_{oc} to modeled absorbance; this is justified by comparison to literature experimental data, discussed in modeling section. The injected electrons contribute to a current within the semiconductor, facilitating charge imbalance at the alternating metal-semiconductor interfaces. The charge imbalance results in a measured V_{oc}, and hence a 3 dB cutoff in V_{oc} indicates the presence of a photonic band gap at the wavelength of the incident monochromatic light. We present a study of photonic band gaps in the SPP dispersion relation and their dependence on variations in the device geometry. Alternative explanations for the observed cutoff based on optical diffraction exist, and further evidence is needed to confirm our understanding that the cutoff arises from an upper band edge. Computationally and experimentally observing a corresponding lower band edge will be a topic of future work.

II. Nanolithographic Metallic Grating

Figure 1 outlines the nanolithographic metallic grating device and the characterization technique. Figure 1(a) represents a top view of the Au grating on n-Si substrate. The 1D periodicity W, leading to photonic band gaps, lies along the vertical direction of Fig. 1(e). Figure 1(b-c) show the optical and electrical aspects of the experiment, while Fig. 1(d) shows a simplified picture of the resonance at the upper-band-edge (λ_+) with electric field lines shown in red. Monochromatic light used in the experiment is stepped at 10 nm wavelength increments and is unpolarized. Parameters W, L, and T define the device period, metal cross-section length and metal thickness respectively, and are discussed in more detail below. Parameter values $W = 470$ nm, $L = 187$ nm, and $T = 50$ nm were used in the initial model and experimental device. The present grating design is similar to previous approaches for THz detectors, yet can omit the voltage biasing [22].

III. Modeling

The spectral response of the MSM structure was calculated by finite element modeling (FEM) using COMSOL Multiphysics. Plasmonic gratings can be effectively modeled using FEM to solve Maxwell's equations [23]. A two-dimensional (2D) modeling domain was defined according to parameters W, L, and T as defined in the introduction and depicted in Fig. 2(a). The modeling domain is comprised of three regions: an upper air region (light gray), a central metallic Au region (yellow) representing a cross-section of one electrode, and a lower semiconducting Si region (dark gray). Au and Si regions use literature material properties while the upper air region uses free space permittivity and permeability values [21], [24]. A periodic boundary condition is imposed on left and right boundaries simulating an infinite 1D structure; top and bottom boundaries are perfectly matched layers to prevent reflection at the boundary; monochromatic light is incident from above, normal to the patterned surface. Incident light is p-polarized. Transmitted power measured at the bottom of the modeling domain is approximately zero confirming that the modeled Si region is sufficiently thick. The sum of the modeled transmittance, absorbance, and reflectance was confirmed to be unity for all modeled results. Figure 2(b) depicts the magnetic field intensity profile at an incident wavelength of 470 nm, with false color representing the magnetic field. Note the spatially oscillating wave in intensity that has the same periodicity as the grating. Absorbance (α) denotes the integral of the power loss density (Q) within the applicable region divided by the incident light power (P_0) and is expressed as:

$$\alpha = \frac{1}{P_0} \iiint_V Q \, dx \, dy \, dz \tag{2}$$

Figure 3 shows α for a thin film and grating structure and experimental V_{oc} for a device using parameters $W = 470$ nm,

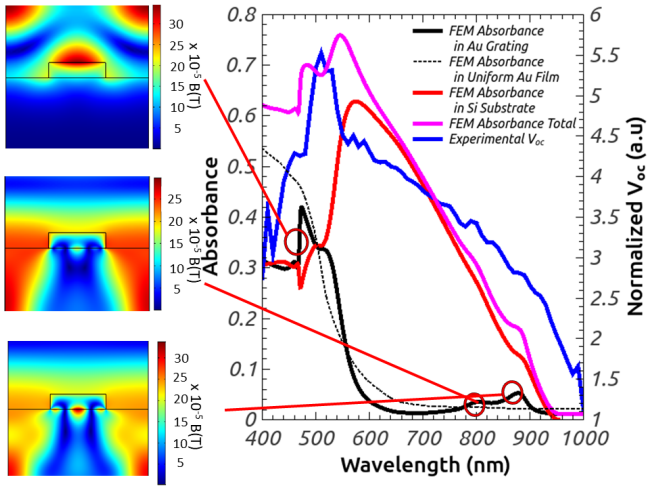

Fig. 3. Comparison of FEM absorbances (left axis) and experimental V_{oc} (right axis). The incremental incident wavelength step in experimental results is 10 nm. FEM absorbances are calculated in a grating structure with geometrical parameters $W = 470$ nm, $L = 187$ nm and $T = 50$ nm (Dashed black line: absorbance in a uniform metal film; solid black line: absorbance in the metal grating; solid red line: absorbance in Si beneath the grating; solid pink line: the sum total absorbance in the metal grating and Si). FEM absorbance for a uniform thin film is calculated by choosing geometrical parameters $W = 470$ nm, $L = 470$ nm and $T = 50$ nm. Note the sharp increase in absorbance of the uniform film below a wavelength of 520 nm due to the interband transition in Au. However, the introduction of the periodic grating cuts off this increase in absorbance. Additionally, two LSP modes are observed in the FEM absorbance at wavelengths 804 nm and 878 nm. Insets show the magnetic field profiles at 470 nm, 804 nm, and 878 nm as indicated.

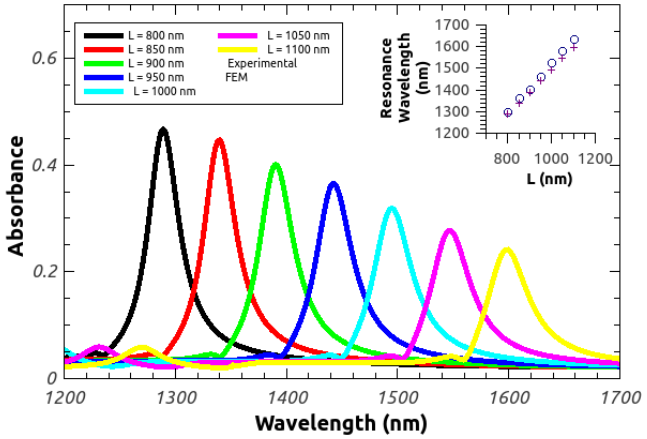

Fig. 4. Comparison of our FEM modeled metallic absorbance to literature measured experimental photoresponse [11]. Modeled absorbances are shown for 7 values of L as listed, with $W = L + 250$ nm and $T = 200$ nm. Inset shows the agreement with experimental photoresponse of devices with identical geometrical parameters.

$L = 187$ nm and $T = 50$ nm (Dashed black line: absorbance in a uniform metal film; solid black line: absorbance in the metal grating; solid red line: absorbance in Si beneath the grating; solid pink line: the sum total absorbance in the metal grating and Si). FEM absorbance in a uniform thin film is calculated by choosing geometrical parameters $W = 470$ nm, $L = 470$ nm and $T = 50$ nm. From the inset magnetic field intensity profiles, we see that a long range SPW is indicated at 470 nm, whereas LSP are indicated on the Au-Si interface at both 804 nm and 878 nm. Incident radiation is swept over the visible spectrum from wavelengths 400 nm to 1000 nm. Results of the model suggest maxima in the total absorbance, in agreement with a maximum in V_{oc} at approximately 500 nm, as illustrated in Fig. 3. The increased α at wavelengths shorter than 500 nm can be explained by Joule loss in the Au. However, a similar behavior is observed in a modeled Ag structure indicating that the observed maxima in α is at least in part plasmonic. High α is an indication of hot carrier generation. We understand the measured V_{oc} to be primarily caused by both the generation of hot carriers in the metal grating, and electron-hole pair creation in the Si. Note that the total absorbance displays α contributions from both Au and Si regions. However, a more detailed investigation than aimed in the present work, is required to determine the correct relative weighting of the two effects. The correct weighting may be determined *a priori* through a method of nonequilibrium scattering in space and energy [25] and will be the focus of continuing work. The validity of the FEM is further confirmed by comparison with experimental photoresponse from the literature in Fig. 4 [11]. Modeled absorbance is shown for $L = 800$ nm, 850 nm, 900 nm, 950 nm, 1000 nm, 1050 nm, 1100 nm, and $W = L + 250$ nm and $T = 200$ nm. The agreement between our FEM modeled absorbance (crosses) and the measured photoresponse (circles) of Ref. [11] is depicted in Fig. 4 inset. These resonance modes are understood to originate from LSPs in the individual grating finger cross sections. Our device may be compared to the device described in Sobhani *et al.* because both devices utilize hot electron injection to generate a photoresponse. The validity of the model is additionally corroborated by comparison to optical transmittance experiments. A 50 nm thick Au film was deposited on a glass microscope slide cover using an identical method to the grating device. The transmittance of the Au-coated glass slide cover was measured using UV-visible spectrometry. Transmittance was modeled for a uniform 50 nm Au film on a glass substrate using the same modeling procedures outlined above. Strong qualitative agreement between our FEM transmittance and our measured transmittance can be seen in Fig. 5. The quantitative difference is likely due to the difference in thickness of the glass in the experimental device ($\approx$160 μm) and model ($\approx$0.5 μm). The maximum in transmittance at $\approx$500 nm would be due to coupling of SPWs at respectively the air-Au interface and the glass-Au interface (analogous to electron tunneling through an oxide interface). Evidence of this plasmon coupling can be observed in Fig. 5 inset.

IV. Results

Experimental and FEM data indicate a maximum in V_{oc} centered at an incident wavelength approximately 500 nm. Generation of V_{oc} is a multi-step process. Plasmons may in general decay along a number of pathways. They may reradiate a photon, they may generate a hot electron, or they may transfer energy to a crystal lattice. Geometrical and material properties affect the likelihood of plasmons decaying along any given pathway [25]. Because FEM results are

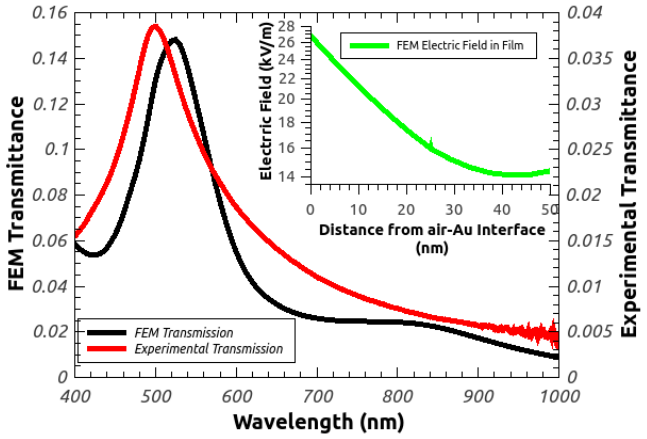

Fig. 5. FEM modeled transmittance, and experimentally measured transmittance of 50 nm Au on glass. The quantitative difference between the modeled and experimental transmittance can be attributed to the FEM model domain not including the total thickness of the glass. Inset shows the evanescent electric field from the air-metal interface. The "turn-around" positive slope between 45 nm and 50 nm (near the metal-glass interface) may be indicative of the presence of a surface plasmon wave at the metal-glass interface. The small spike in electric field occurring at 25 nm in the exact center of the grating cross section is believed to be an artifact.

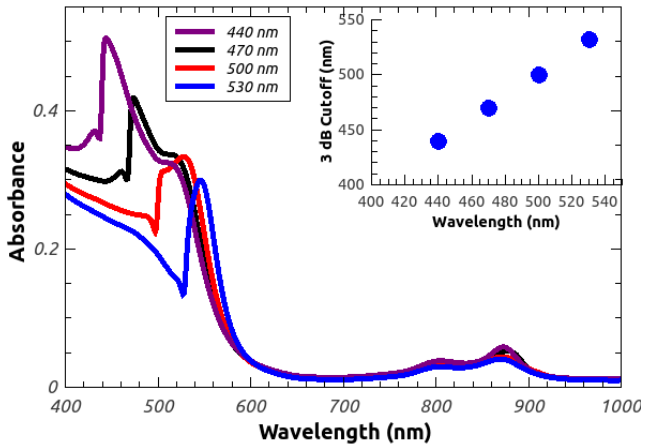

Fig. 6. Dependence of the upper-band-edge (λ_+) on geometrical parameter W. The FEM modeled metallic absorbances for W = 440 nm, 470 nm, 500 nm, 530 nm, and, L = 187 nm and T = 50 nm are shown. The inset shows the linear dependence of upper-band-edge vs periodicity. Note that the wavelengths of LSP resonances are unaffected by parameter W.

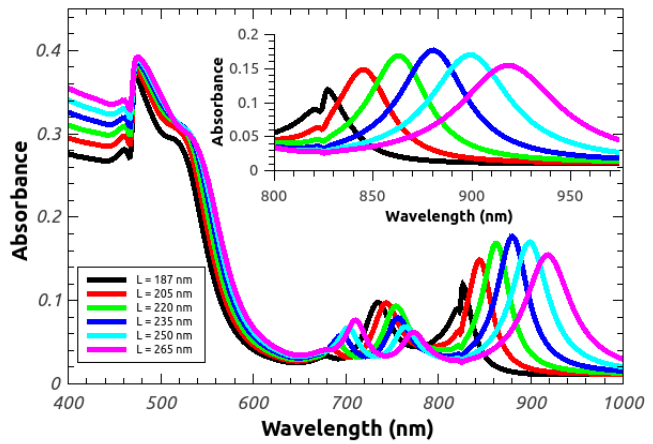

Fig. 7. Dependence of the upper-band-edge (λ_+) on geometrical parameter L. The FEM modeled metallic absorbance for L = 187 nm, 205 nm, 220 nm, 235 nm, 250 nm, 265 nm, and W = 470 nm and T = 50 nm are shown. The inset shows the a magnified view of the LSP resonance mode with the longest wavelength. Note that the upper-band-edge (λ_+) is unaffected by parameter L.

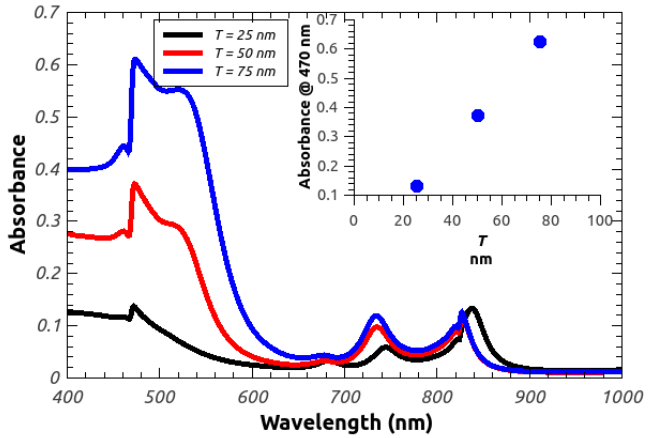

Fig. 8. Dependence of the upper-band-edge (λ_+) on geometrical parameter L. The FEM modeled metallic absorbance for T = {25 nm, 50 nm, 75 nm}, L = 187 nm and W = 470 nm are shown. The inset shows a zoomed in view of the LSP resonances.

obtained in steady-state, reradiated photons present themselves as electromagnetic field oscillations, and do not contribute to the modeled absorbance. The FEM absorbance can then be understood to be entirely due to hot carrier generation and phonon mode excitation. These can be due to intraband excitations or interband transitions. Interband transitions can excite hot holes in addition to hot electrons. The electronic response is dependent not only on the hot carrier generation, but also on the likelihood that hot carriers will reach the Au-Si interface. This is dependent on not only the distance from the interface where the hot carrier is generated, but also the likelihood of electron-electron and electron-phonon scattering. Hot electron injection as a primary contributor to V_{oc} is in agreement with the literature [25]–[27]. A more rigorous description of hot electron generation in plasmonic resonance structures such as those studied in this paper may be found in Jermyn *et al.* [25]. Electron-hole creation in the Si substrate is also a non negligible contributor to V_{oc}. However, this is well understood and hence we emphasize the metallic contribution. The metallic gratings discussed are understood to have two types of plasmonic effects: SPW effects where wavelengths shorter than the upper-band-edge (λ_+) are suppressed, and LSP effects where a dipole moment is excited along the length of the finger cross section. Three design parameters W, L and T affect the behavior of SPW and LSP uniquely. Figure 6 shows the upper-band-edge(λ_+) dependence on W. The inset shows the linear relationship between upper-band-edge (λ_+) and the period. The two LSP resonance modes occur at the same wavelength independent of W. This supports the understanding that the cutoff is due to the long range aspect of the SPW while the resonances at 804 nm and 878 nm are due to LSP resonances, and are thus primarily affected by L and T. Figure 7 shows the L dependence of the absorbance, which further supports this picture. Two identified LSP resonance modes shift towards longer wavelengths with longer L, showing a linear trend. Figure 8 shows that the overall spectral

response is independent of T. However, the magnitude is affected by T, due to both the increase in the total volume of the absorbing material, as well as the decoupling of surface plasmons at the Au-Si interface and the Au-air interface. The Au width L has the most significant effect on LSP. As T increases, the peak wavelength for the short-wavelength LSP moves slightly, while the absorbance increases.

V. Conclusion

A study is presented to determine the spectral behavior of a nanofabricated metal-semiconductor-metal metallic grating, based on geometrical parameters. Finite element modeling was used to determine the expected spectral response of the nanostructured surface. Strong agreement exists between the calculated absorbance of the metallic structure and the measured photoresponse, corroborating the model. Electrical measurements may be used as a probe of photonic band gaps, providing a necessary step forward in the integration of optics with electronics. The electronic technique is not limited to detecting photonic band gaps but can be employed in the study of any plasmonic resonant structured surfaces. We observe the upper-band-edge (λ_+) resulting from what is understood to be a photonic band gap occurring at a wavelength approximately equal to the period. Lower intensity, but more geometrically controllable LSP occur at longer wavelengths. Two LSP modes are observed, with locations strongly dependent on L and the height of the shorter wavelength mode strongly dependent on T. The L dependence is understood to be due to the dipole moment of the finger cross section, and the T dependence originates from a decoupling effect between plasmons on the Si-Au and air-Au interfaces. The possibility thus lies open to engineer future device designs to exhibit wavelength selectivity by tuning geometrical parameters. Far-field effects and more rigorous computations of hot carrier injection using a method of nonequilibrium scattering in space and energy. [25] for the study of nanolithographic structured surfaces will form the focus of future work.

Acknowledgment

The authors wish to acknowledge T. Asryan for contributions to COMSOL models.

References

[1] A. Poddubny, I. Iorsh, P. Belov, and Y. Kivshar, "Hyperbolic metamaterials," *Nature Photon.*, vol. 7, no. 12, p. 948, Dec. 2013.
[2] P. Li *et al.*, "Infrared hyperbolic metasurface based on nanostructured van der Waals materials," *Science*, vol. 359, no. 6378, pp. 892–896, Feb. 2018.
[3] A. A. High *et al.*, "Visible-frequency hyperbolic metasurface," *Nature*, vol. 522, no. 7555, pp. 192–196, Jun. 2015.
[4] A. J. Hoffman *et al.*, "Negative refraction in semiconductor metamaterials," *Nature Mater.*, vol. 6, pp. 946–950, Dec. 2007.
[5] S. Yoo, S. Lee, and Q.-H. Park, "Loss-free negative-index metamaterials using forward light scattering in dielectric meta-atoms," *ACS Photon.*, vol. 5, no. 4, pp. 1370–1374, Apr. 2018.
[6] I. V. Shadrivov, A. B. Kozyrev, D. W. van der Weide, and Y. S. Kivshar, "Tunable transmission and harmonic generation in nonlinear metamaterials," *Appl. Phys. Lett.*, vol. 93, no. 16, Oct. 2008, Art. no. 161903.
[7] J. T. Collins, D. C. Hooper, A. G. Mark, C. Kuppe, and V. K. Valev, "Second-harmonic generation optical rotation solely attributable to chirality in plasmonic metasurfaces," *ACS Nano*, vol. 12, no. 6, pp. 5445–5451, Jun. 2018.
[8] W. L. Barnes, T. W. Preist, S. C. Kitson, J. R. Sambles, N. P. K. Cotter, and D. J. Nash, "Photonic gaps in the dispersion of surface plasmons on gratings," *Phys. Rev. B, Condens. Matter*, vol. 51, no. 16, pp. 11164–11167, Apr. 1995.
[9] W. L. Barnes, T. W. Preist, S. C. Kitson, and J. R. Sambles, "Physical origin of photonic energy gaps in the propagation of surface plasmons on gratings," *Phys. Rev. B, Condens. Matter*, vol. 54, no. 9, pp. 6227–6244, Sep. 1996.
[10] W. L. Barnes, A. Dereux, and T. W. Ebbesen, "Surface plasmon subwavelength optics," *Nature*, vol. 424, no. 6950, pp. 824–830, Aug. 2003.
[11] A. Sobhani *et al.*, "Narrowband photodetection in the near-infrared with a plasmon-induced hot electron device," *Nature Commun.*, vol. 4, no. 1, p. 1643, Jun. 2013.
[12] R. Ritchie, E. Arakawa, J. Cowan, and R. Hamm, "Surface-plasmon resonance effect in grating diffraction," *Phys. Rev. Lett.*, vol. 21, no. 22, pp. 1530–1533, Nov. 1968.
[13] J. A. Porto, F. J. García-Vidal, and J. B. Pendry, "Transmission resonances on metallic gratings with very narrow slits," *Phys. Rev. Lett.*, vol. 83, no. 14, pp. 2845–2848, Oct. 1999.
[14] Q. Cao and P. Lalanne, "Negative role of surface plasmons in the transmission of metallic gratings with very narrow slits," *Phys. Rev. Lett.*, vol. 88, no. 5, Jan. 2002, Art. no. 057403.
[15] C. Girard, "Near fields in nanostructures," *Rep. Prog. Phys.*, vol. 68, no. 8, pp. 1883–1933, Aug. 2005.
[16] W. Rieger, J. J. Heremans, H. Ruan, Y. Kang, and R. Claus, "Yagi-uda nanoantenna enhanced metal-semiconductor-metal photodetector," *Appl. Phys. Lett.*, vol. 113, no. 2, Jul. 2018, Art. no. 023102.
[17] J. Yoon, G. Lee, S. H. Song, C.-H. Oh, and P.-S. Kim, "Surface-plasmon photonic band gaps in dielectric gratings on a flat metal surface," *J. Appl. Phys.*, vol. 94, no. 1, pp. 123–129, Jul. 2003.
[18] A. V. Zayats, I. I. Smolyaninov, and A. A. Maradudin, "Nano-optics of surface plasmon polaritons," *Phys. Rep.*, vol. 408, nos. 3–4, pp. 131–314, Mar. 2005.
[19] E. Yablonovitch, "Photonic band-gap structures," *J. Opt. Soc. Amer. B, Opt. Phys.*, vol. 10, no. 2, pp. 283–295, 1993.
[20] M. Javaid and T. Iqbal, "Plasmonic bandgap in 1D metallic nanostructured devices," *Plasmonics*, vol. 11, no. 1, pp. 167–173, Feb. 2016.
[21] P. B. Johnson and R. W. Christy, "Optical constants of the noble metals," *Phys. Rev. B, Condens. Matter*, vol. 6, no. 12, pp. 4370–4379, Dec. 1972.
[22] T. Hattori, K. Egawa, S.-I. Ookuma, and T. Itatani, "Intense terahertz pulses from large-aperture antenna with interdigitated electrodes," *Jpn. J. Appl. Phys.*, vol. 45, no. No. 15, pp. L422–L424, Apr. 2006.
[23] S. K. Gray, "Theory and modeling of plasmonic structures," *J. Phys. Chem. C*, vol. 117, no. 5, pp. 1983–1994, Feb. 2013.
[24] D. T. Pierce and W. E. Spicer, "Electronic structure of amorphous Si from photoemission and optical studies," *Phys. Rev. B, Condens. Matter*, vol. 5, no. 8, pp. 3017–3029, Apr. 1972, doi: 10.1103/PhysRevB.5.3017.
[25] A. S. Jermyn, G. Tagliabue, H. A. Atwater, W. A. Goddard, P. Narang, and R. Sundararaman, "Transport of hot carriers in plasmonic nanostructures," *Phys. Rev. Mater.*, vol. 3, no. 7, Jul. 2019, Art. no. 075201, doi: 10.1103/PhysRevMaterials.3.075201.
[26] M. W. Knight, H. Sobhani, P. Nordlander, and N. J. Halas, "Photodetection with active optical antennas," *Science*, vol. 332, no. 6030, pp. 702–704, May 2011.
[27] C. Zhang *et al.*, "Thermodynamic loss mechanisms and strategies for efficient hot-electron photoconversion," *Nano Energy*, vol. 55, pp. 164–172, Jan. 2019.

William T. Rieger, Jr., received the bachelor's degree in physics from Rowan University in 2014 and the M.Sc. degree from Virginia Tech in 2018, where he is currently pursuing the Ph.D. degree with the Professor Heremans's Group. He has performed Undergraduate Research with the National High magnetic Field Laboratory, Los Alamos, NM, USA, and has been a recipient of the William E. Hassinger and James A. Jacobs Graduate Fellowships. He is also a part-time Researcher with NanoSonic Inc., with a significant financial interest in the latter. His research interests include experimental mesoscopic physics with emphasis on engineering applications, nanoscale optoelectronic structures, and nanofabrication techniques.

Yuhong Kang received the B.Sc. degree in optics from the Huazhong University of Science and Technology, China, in 1991, and the Ph.D. degree in semiconductor physics from the Department of Electrical Engineering, Virginia Polytechnic Institute and State University, USA, in 2015. She is currently the Lead Nanoelectronics Scientist with NanoSonic Inc., USA, where she has led multiple projects involving nonlinear optical effects in fibers, high-frequency pressure sensors, wireless networked sensors, and non-volatile memory devices. Her research interests also include theoretical analysis and experimental demonstration of quantized and partial quantized conductance effects in organic-inorganic-hybrid materials.

Jean J. Heremans received the bachelor's degree in applied sciences from the University of Leuven, Belgium, in 1987, the master's degree in arts from Princeton University in 1989, and the Ph.D. degree from Princeton University in 1994. He was a Researcher with Florida State University and the National High Magnetic Field Laboratory, a Staff Scientist with Emcore Corporation, and the Director of the Nanoscale and Quantum Phenomena Institute, Ohio University. He is currently a Professor of physics with Virginia Tech. His research interests include experimental mesoscopic physics, nanoscale magnetic, optical and electronic structures, electronic magnetotransport phenomena, nanofabrication, and spinand quantum phase coherence phenomena.

Hang Ruan received the B.Sc. degree in optics from the Huazhong University of Science and Technology, China, in 1991, and the Ph.D. degree in optoelectronics from the Xi'an Institute of Optics and Precision Mechanics, Chinese Academy of Sciences, China, in 1996. He is currently the Vice President with NanoSonic Inc., USA, where he also leads the Sensors and Systems Division. He is also an Adjunct Professor with the Department of Mechanical Engineering, Virginia Polytechnic Institute and State University, USA. His principal research interests are in the quantum electronics and smart material related fields, such as micro/nano/RF photonics, semiconductor-based micro/nano membrane, fiber optic/bio/nano sensors, molecular self-assembly, flexible electronics, and other nano-scale devices.